Int. J. Heat Mass Transfer. Vol. 33, No. 2, pp. 319–329, 1990
Printed in Great Britain

0017–9310/90 $3.00+0.00

Coupled radiation and laminar mixed convection in an absorbing and emitting real gas mixture along a vertical plate

L. ZHANG, A. SOUFIANI, J. P. PETIT and J. TAINE
Laboratoire d'Energétique Moléculaire et Macroscopique, Combustion, du CNRS et de l'ECP, Ecole Centrale des Arts et Manufactures, 92295 Châtenay–Malabry Cedex, France

(*Received* 6 *December* 1988 *and in final form* 4 *April* 1989)

Abstract—The radiation transfer part is treated by the application of a random statistical narrow-band model and the Curtis–Godson approximation. An implicit finite-difference technique, developed for this study is used to solve the mass, momentum and energy conservation equations in a coupled manner. Excellent agreement between our finite-difference solutions and those of other authors are obtained for pure natural convection, pure forced convection and mixed convection without radiation. The investigation of the boundary conditions at infinity shows that the radiation penetration length at atmospheric pressure is of the order of one pure H_2O equivalent metre, which is one order of magnitude larger than the boundary layer thickness for mixed convection without fluid radiation. Comparison of results with and without radiation in various conditions shows that fluid radiation enhances the effect of buoyancy forces, increases temperature, velocity, and conductive heat transfer at the wall, but decreases the wall radiative heat flux. A dimensionless parameter R is introduced in order to enable a crude estimation of wall conductive flux enhancement due to radiation.

1. INTRODUCTION

COUPLED radiation and mixed convection heat transfer arise in many engineering devices (such as nuclear reactors and solar energy systems) where the interaction of radiation, natural and forced convection becomes significant. Coupled radiation and external convection over surfaces is a complex problem, since the fluid radiation induces an additional difficulty for the boundary conditions at infinity; in fact the radiation penetration length is much larger than the conventional external convection boundary layer thickness. A limited amount of work is only available in the area of radiation with natural convection [1–6] and with forced convection [7, 8] along a vertical plate. Among these studies a wide range of numerical techniques has been used to solve the governing equations: the singular perturbation technique [1], the approximate integral method [2], local non-similarity techniques [3, 4, 6] and finite-difference methods [5, 8].

Boundary conditions at infinity have been discussed by Hasegawa *et al.* [3] in their analytical and experimental studies on simultaneous radiative and natural convective heat transfer along a vertical plate. They concluded that the dimensionless temperature and velocity are not zero for large η (dimensionless pseudo-similarity variable for natural convection). Although the validity of the boundary layer approximation for large η has to be submitted to further examination, the solutions in the vicinity of the heating wall are nevertheless acceptable. The boundary conditions at infinity were also treated by Cess [7] in a study of coupled radiation and forced convection in boundary layer flow along a flat plate. The flow region was divided into two layers: the conventional thermal boundary layer which is optically thin, and an adjacent radiation layer which is not optically thin and within which conduction effects were neglected.

Most previous authors used a gray gas assumption [1–5, 8], and the optically thin [2, 7] and thick [1, 2, 5] limits were also frequently considered. Cess [7] treated a non-gray gas for which the absorption coefficient, depending on the wavelength, was assumed to be independent of temperature. Novotny *et al.* [6] formulated the radiation term using the total band absorption based on the exponential wide-band model. However, more accurate radiative models such as the exponential wide-band model [9–12] and the random statistics narrow-band model [13] have been more frequently applied to radiation coupled with internal natural or forced convection heat transfer.

The present work investigates coupled radiation and mixed convection heat transfer along a vertical isothermal plate. To our knowledge there has not been any reported study concerning coupled radiation and mixed convection heat transfers. The usual boundary layer equations involving a radiative dissipation term are introduced. The absorbing and emitting fluid is modelled by a random statistical narrow-band model and the Curtis–Godson approximation (Section 2). The radiative transfer part is treated using a method similar to that used in refs. [13, 14]. An implicit finite-difference technique, a marching solution procedure and an extended tridiagonal matrix algorithm (E-TDMA) are applied to solve the mass, momentum and energy conservation equations in a coupled

NOMENCLATURE

a	thermal diffusivity
c_p	thermal capacity
d	ratio of geometrical series
g	gravitational acceleration
Gr_x	local Grashof number, $g\beta(T_w-T_\infty)x^3/\nu^2$
h_C, h_R	local conductive and radiative transfer coefficients
I	radiative intensity
I^b	blackbody radiative intensity
I^i	incident radiative intensity
$\overline{k_\nu}$	mean line intensity to spacing ratio inside $\Delta\nu$
l	elementary column length
m	normal grid spacing number
n	axial grid spacing number
Nu_x	local Nusselt number for mixed convection without radiation, hx/λ
P	total pressure
q_c	conductive heat flux
q^R	radiative heat flux
R	dimensionless parameter
R_q	relative enhancement of conductive flux, $(q_c-q'_c)/q'_c$
Re_x	local Reynolds number, $u_\infty x/\nu$
T	temperature
u	axial velocity component
v	normal velocity component
x	axial coordinate
x_{H_2O}	molar fraction of water vapour
y	normal coordinate.

Greek symbols

α	gas layer absorptivity
β	coefficient of thermal expansion
$\overline{\beta_\nu}$	mean line width to spacing ratio
ε	emissivity
η	dimensionless pseudo-similarity variable
θ	dimensionless temperature, $(T-T_\infty)/(T_w-T_\infty)$
λ	thermal conductivity
μ	cosine in radiative developments
ν	kinematic viscosity
$\Delta\nu$	spectral range
ρ	density
τ	transmissivity.

Subscripts

w	wall
ν	spectral quantity
∞	ambient.

manner. The solution procedure is detailed in Section 3. The boundary conditions at infinity are studied either from the temperature and velocity profiles or from the radiative dissipation distributions (Section 3.1). Our finite-difference solutions for mixed convection without fluid radiation are compared with those of other authors in Section 4.2. Different controlling parameters are studied for coupled radiation with mixed convection, the results on temperature and velocity profiles and on heat transfer coefficients are reported in Section 4.3 and a discussion follows.

2. BASIC FORMULATIONS

Consider coupled radiation and mixed convection along a vertical plate, at a temperature T_w and with an emissivity ε_w, immersed in an absorbing, emitting but non-scattering gas mixture at temperature T_∞ with an assisting external flow at u_∞ (Fig. 1).

The following assumptions are introduced:

(1) two-dimensional, steady-state laminar flow;

(2) the fluid has constant physical properties except for density in the buoyancy term and for radiative properties; the Boussinesq approximation is employed;

(3) the usual boundary layer assumptions are made;

(4) the radiative dissipation in the x-direction is negligible in comparison with that in the y-direction, and the radiative flux at a given location x depends only on the temperature profile at the same x location;

(5) the wall is diffuse but not necessarily gray.

As pointed out in refs. [10, 13], a dimensionless treatment of the governing equations has a very limited utility in the case of realistic gas band radiation. The mass, momentum and energy conservation equations are, under the above assumptions, written as follows:

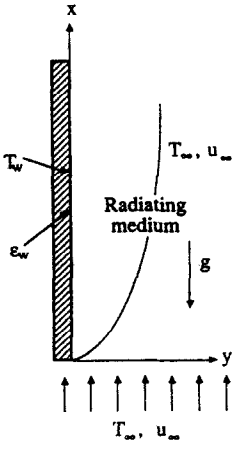

FIG. 1. Geometry and coordinate system.

$$\frac{\partial u}{\partial x}+\frac{\partial v}{\partial y}=0 \tag{1}$$

$$u\frac{\partial u}{\partial x}+v\frac{\partial u}{\partial y}=\nu\frac{\partial^2 u}{\partial y^2}+g\beta(T-T_\infty) \tag{2}$$

$$u\frac{\partial T}{\partial x}+v\frac{\partial T}{\partial y}=a\frac{\partial^2 T}{\partial y^2}-\frac{1}{\rho c_p}\frac{\partial q^R}{\partial y}. \tag{3}$$

In equation (3), q^R is the radiative flux per unit area in the y-direction

$$q^R=\sum_{\text{spectrum}}\left[2\pi\left(\int_0^1 \overline{I_\nu}\mu\,d\mu-\int_0^{-1}\overline{I_\nu}\mu\,d\mu\right)\right]\Delta\nu \tag{4}$$

where μ is the cosine of the angle between the direction of radiative intensity and the Oy axis; $\overline{I_\nu}$ the radiative intensity averaged in the spectral range $[\nu-\Delta\nu/2, \nu+\Delta\nu/2]$, which is given, for the non-scattering medium, by the following equation:

$$\overline{I_\nu(s)}=\overline{I_\nu(0)\tau_\nu(0,s)}+\int_0^s I_\nu^b(s')\frac{\partial\overline{\tau_\nu(s',s)}}{\partial s'}ds' \tag{5}$$

where $I_\nu(0)$, $I_\nu^b(s')$ are respectively the spectral radiative intensity at the boundary and the blackbody intensity related to the temperature $T(s')$; $\overline{\tau_\nu(s',s)}$ the mean transmissivity of an elementary column gas medium from s' to s. The high resolution spectral correlations, which appear in $\overline{\tau_\nu(s',s)}$ should be taken into account; a comparison of spectral correlated and non-correlated radiative transfer calculations [15] shows that non-correlated models may lead to inaccurate qualitative results. In the present investigation, we account for the spectral correlations. A random statistical narrow-band model due to Goody [16] with an exponential-tailed inverse line-strength distribution [17] is used to calculate the radiative transmissivities of the absorbing and emitting gas medium. The transmissivity of a homogeneous column of length l, due to the gas species i, averaged over the spectral range $[\nu-\Delta\nu/2, \nu+\Delta\nu/2]$, is given by

$$\overline{\tau_\nu^i}=\exp\left[-\frac{\overline{\beta_\nu}}{\pi}\left(\left(1+\frac{2\pi x_i P l\overline{k_\nu}}{\overline{\beta_\nu}}\right)^{1/2}-1\right)\right] \tag{6}$$

where x_i and P are the molar fraction of the absorbing species i and the total pressure, respectively. $\overline{k_\nu}$, $\overline{\beta_\nu}$ are the spectral parameters generated either from experimental spectra [18] or from a line-by-line calculation [14, 19–21]. For a non-isothermal or non-homogeneous column the Curtis–Godson approximation [22, 23], which leads to very accurate results, is applied to transform such a column into an equivalent homogeneous column.

The boundary conditions for equations (1)–(3) are

$$u=v=0, \qquad T=T_w \quad \text{at } y=0 \tag{7}$$

$$u\to u_x, \qquad T\to T_\infty \quad \text{at } y\to\infty \tag{8}$$

$$u=u_x, v=0, \quad T=T_\infty \quad \text{at } x=0. \tag{9}$$

For the radiative transfer equation (5), the boundary conditions are given as

Table 1. Present calculations with different discretization numbers (m,n) compared with the results of ref. [28] for mixed convection without radiation and $Pr=1$

Gr_x/Re_x^2	$Nu_x/\sqrt{(Re_x)}$ Present results (m,n) (20×100)	(40×200)	(80×400)	Ref. [28]
0.2900	0.4030	0.3940	0.3905	0.3864
0.4210	0.4162	0.4093	0.4068	0.4054
0.5300	0.4279	0.4219	0.4197	0.4189
0.6290	0.4349	0.4303	0.4290	0.4297
0.7240	0.4425	0.4385	0.4378	0.4392
1.2010	0.4783	0.4766	0.4764	0.4834
1.7790	0.5099	0.5101	0.5111	0.5175
2.5920	0.5457	0.5478	0.5499	0.5546
3.8730	0.5882	0.5928	0.5962	0.6012
6.1690	0.6485	0.6556	0.6601	0.6644
11.0660	0.7348	0.7453	0.7515	0.7582
24.9800	0.8777	0.8924	0.9007	0.9179
99.9950	1.2319	1.2567	1.2697	1.2829

$$\overline{I_\nu}=\varepsilon_w I_\nu^b(T_w)+(1-\varepsilon_w)\overline{I_\nu^i} \quad \text{at } y=0 \tag{10}$$

$$\overline{I_\nu}=I_\nu^b(T_\infty) \quad \text{at } y\to\infty \tag{11}$$

where $\overline{I_\nu}$ and $\overline{I_\nu^i}$ are the outgoing and incident radiative intensities at the boundaries, respectively.

The radiative flux depends on the temperature field, however the temperature and velocity fields are modified by the gas radiation. Thus, an iterative solution scheme is introduced: the mass, momentum and energy conservation equations (1)–(3) and radiative transfer equation (5) are alternately solved; the radiative flux and dissipation are deduced from the previously obtained temperature field and then used to adjust the temperature field by solving equations (1)–(3). The final results are obtained when the maximum changes of the temperature and radiative flux are small enough.

3. SOLUTION PROCEDURE

Equations (1)–(3) together with boundary conditions (7)–(9) are solved using an implicit finite-difference scheme. Second-order derivatives are written in central differences; forward differences are used for first-order derivatives in y, and backward differences for x derivatives. As equations (2) and (3) are parabolic, a marching solution procedure in the x-direction may be applied.

The flow region is divided into a grid with n and m spacings in the x- and y-directions. A constant mesh size is used for x, namely $\Delta x=x_{max}/n$, where x_{max} is considered to represent the total height of the plate. The value of x_{max} is chosen to correspond to a Grashof number $Gr_{x_{max}}=9.6\times10^7$, i.e.

$$x_{max}=[9.6\times10^7\nu^2/g\beta(T_w-T_\infty)]^{1/3}.$$

The mesh size for y is a geometrical progression of ratio d defined by $\Delta y_m/\Delta y_1=d^{m-1}=100$. Different values of n and m were investigated in various conditions, Table 1 shows the results calculated with different values of m and n in the case of mixed con-

vection without fluid radiation. When the values of m and n are increased from (40, 200) to (80, 400), the variations of local Nusselt number are smaller than 1%. In the following computations, the values of $(m, n) = (40, 200)$ are chosen. The radiative transfer calculation is based on a different grid, generated from the above one. $M_R = 20$ spacings in the y-direction is large enough; doubling M_R leads to a maximum temperature difference less than $10^{-3}(T_w - T_\infty)$. The spacing size Δy^R for the radiative transfer solution is the sum of two adjacent ones for the coupled transfer calculation when $m = 40$. Linear interpolation or extrapolation are employed for the transformation of radiative dissipation between the two grids. The resolution of the radiative transfer equation (integral equation) requires a smaller grid number than momentum and energy equations (partial differential equation). This is due to the different mathematical nature of these equations.

Non-linear equations (1)–(3) are coupled to each other through temperature and velocity. The quasi-linearization technique is used to linearize equations (2) and (3), except for the radiative dissipation term in equation (3), because it is given from an iterative solution. A second iterative scheme is necessary for the solution of the linearized equation system deduced from equations (1)–(3). By using a method similar to that in Blottner [24], the tridiagonal matrix algorithm (TDMA) has been extended, in the present work, to solve the governing equations (mass, momentum and energy conservation equations) in a coupled manner. Our extended method is called E-TDMA [25].

The marching solution procedure starts at $x = 0$ and proceeds step by step until $x = x_{max}$. For each step x, two levels of iteration have to be carried out. The primary iterative loop involves the solution of the system equations (1)–(3) by the application of E-TDMA, using the radiative dissipation distribution issued from the previous second level of iteration. The primary iteration is carried out until convergence is obtained. The change in the dimensionless local temperature $(\theta = (T - T_\infty)/(T_w - T_\infty))$ in each cycle of calculation is determined and when the maximum change is less than 10^{-4}, the solution is considered to have converged. This is verified by the fact that no difference in the results is observed when the convergence criterion is taken to be 10^{-5}. A second level of iteration is performed for radiative transfer: calculations of the radiative flux and dissipation are based on the converged temperature field from the primary iteration. When the maximum change in radiative dissipation is less than 2% of the peak value, the convergence of radiative dissipation is assumed to have been obtained. Dividing the convergence criterion of the radiative dissipation by 2 leads to a difference in dimensionless temperature of less than 0.1%.

The double iteration procedure is initialized at each step x by the temperature, velocity and radiative dissipation profiles at $x - \Delta x$. The initial radiative dissipation at $x = 0$ is taken to be zero.

4. RESULTS AND DISCUSSION

4.1. *Calculation without gas radiation*

Preliminary calculations have been carried out without consideration of the gas radiation over the regimes of natural, forced and mixed convection. The temperature and velocity profiles obtained by our finite-difference method at various x locations are compared with the similarity solution of Ostrach [26] for pure natural convection and with the similarity solution of Blasius flow [27] for pure forced convection. An excellent agreement between our results and the similarity solutions is obtained. The largest deviation in velocities and in temperatures at location x in the range $[x_{max}/10, x_{max}]$ is less than 1% for both cases of pure natural convection and pure forced convection. The same maximal deviation is observed for Nusselt numbers and wall friction coefficients as shown in Table 2. The local Nusselt number for mixed convection flow is compared with the numerical results of Raju *et al.* [28]. Figure 2 shows the variation of $Nu_x/\sqrt{(Re_x)}$ with Gr_x/Re_x^2. Our finite-difference solutions agree well with those of ref. [28].

4.2. *Boundary conditions at infinity*

Coupled radiation and mixed convection calculations are carried out for an air–water vapour mixture. It should be pointed out that there is no difficulty in the application of the present formulations to any other radiating real gas mixture. The thermophysical properties of the air–H_2O mixture are evaluated at a film temperature $(T_w + T_\infty)/2$ by identical formulations to those of ref. [13], which were obtained from refs. [29, 30]. The H_2O absorption bands centred at 2.7, 6.3 μm and the rotational band centred at 20 μm are considered with a spectral resolution $\Delta\nu = 25$ cm^{-1}, and 140 spectral intervals are involved.

A difficulty in the treatment of coupled radiation with external convection over a flat plate is the determination of the distance y_{max}, far away from the plate, which may be considered to be the infinite boundary in equations (8) and (11), since the radiation penetration length is much larger than thermal and dynamic boundary layer thicknesses. For pure natural convection flow along a vertical plate, y_{max} may be evaluated by

$$\eta = \frac{y}{x}\left(\frac{Gr_x}{4}\right)^{1/4} = 5$$

for fluids with a Prandtl number Pr in the range of [0.5, 1.0], which is appropriate for an air–H_2O mixture. For pure forced convection flow with Pr in the same range, a similar equation

$$\eta = \frac{y}{x}\sqrt{(Re_x)} = 5$$

may also be used to estimate the value of y_{max}. When the fluid is a radiating gas, the above equations are no longer valid for determining the value of y_{max}. Most

Table 2. Finite-difference results for pure forced and pure natural convection, compared to similarity solutions (Simil.) for $Pr = 1$

Re_x	$Nu_x/(Re_x)^{1/2}$ Simil.	Our	$C_{f_x}/(Re_x)^{1/2}$ Simil.	Our	Gr_x	$Nu_x/(Gr_x)^{1/4}$ Simil.	Our
1084.0	0.332	0.332	0.664	0.663	4.48×10^6	0.567	0.568
1445.0		0.334		0.667	6.15×10^6		0.567
1807.0		0.331		0.661	8.18×10^6		0.567
2710.0		0.333		0.666	1.06×10^7		0.566
3614.0		0.332		0.665	1.35×10^7		0.566
5421.0		0.334		0.669	1.69×10^7		0.566
7229.0		0.333		0.665	2.07×10^7		0.565
10843.0		0.335		0.670	2.52×10^7		0.565
14458.0		0.333		0.666	3.02×10^7		0.565
21687.0		0.335		0.671	3.59×10^7		0.565
35422.0		0.331		0.662	4.22×10^7		0.565
40483.0		0.332		0.664	4.92×10^7		0.565
45543.0		0.333		0.666	5.69×10^7		0.564
50603.0		0.334		0.667	6.55×10^7		0.564
69399.0		0.330		0.660	7.48×10^7		0.564
80966.0		0.332		0.663	8.50×10^7		0.564
92532.0		0.333		0.665	9.60×10^7		0.564

authors of refs. [1–8] have pointed out that the interaction of radiation and convection widens the boundary layer thickness, yet very few reports can be found for the determination of y_{max} in different physical conditions. In the following we will investigate the value of y_{max}, in the case of coupled radiation and mixed convection along a vertical plate.

At first pure water vapour at $T_\infty = 600$ K and $u_\infty = 1$ m s^{-1} along a vertical isothermal plate at $T_w = 650$ K, $\varepsilon_w = 0.5$ is considered. The governing equations are solved with different values of $y_{max(1,2,3)} = 0.0264$, 0.4528, 0.9055 m, which correspond to values of the dimensionless pseudo-similarity variable for pure natural convection $\eta = 20$, 40, 80 at $x = x_{max}$. The temperature, two components of velocity and radiative dissipation profiles at $x = x_{max}$ are partially shown in Fig. 3 for the three cases. It is observed that the results for temperature T and the axial velocity component u obtained with small and large values of y_{max} differ only in the vicinity of y_{max}.

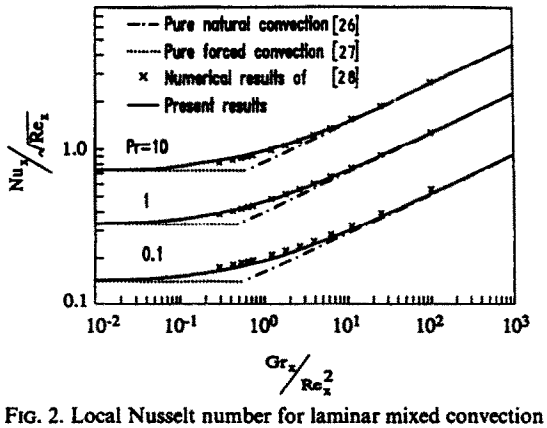

FIG. 2. Local Nusselt number for laminar mixed convection flow without radiation along an isothermal vertical plate.

These differences are due to the conditions imposed at $y = y_{max}$, $T = T_\infty$ and $u = u_\infty$. As no condition at $y = y_{max}$ has been imposed for the normal velocity component v no similar behaviour as for T and u in the vicinity of $y = y_{max}$ are found in the v profile.

The temperature profile obtained with $y_{max} = 0.4528$ m is accurate to within 1% over the temperature difference $T_w - T_\infty$ as shown in Fig. 3. This value of y_{max} to get a 1% accuracy for temperature is generally dependent on the fluid, the temperature level, the temperature difference, the ambient velocity u_∞, etc. In the following we chose the value

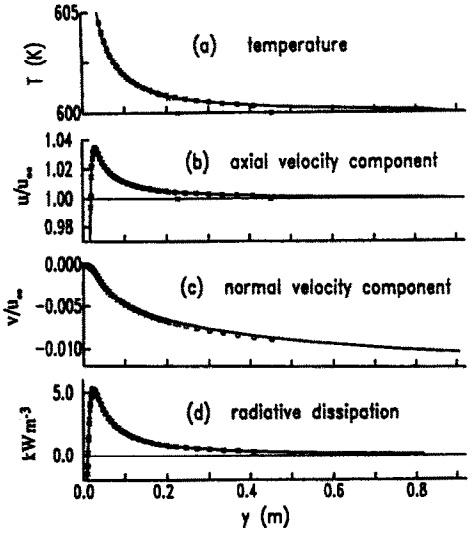

FIG. 3. Temperature, velocity and radiative dissipation profiles at $x = x_{max}$, calculated with different values of y_{max} (×, 0.22464 m; □, 0.4528 m; ——, 0.9055 m) for pure water vapour at conditions $T_w = 650$ K, $\varepsilon_w = 0.5$, $T_\infty = 600$ K, $u_\infty = 1.0$ m s^{-1} (Re_x, Gr_x, Gr_x/Re_x^2 are respectively 1.24×10^4, 9.6×10^7, 0.621).

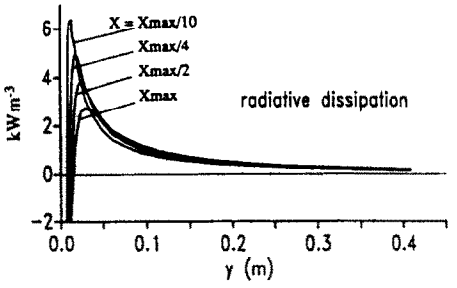

FIG. 4. Radiative dissipation distributions at different locations $x = x_{max}/10$, $x_{max}/4$, $x_{max}/2$, x_{max} for pure water vapour at conditions $T_w = 650$ K, $\varepsilon_w = 0.2$, $T_\infty = 600$ K, $u_\infty = 0.5\ m\ s^{-1}$ (Re_x, Gr_x, Gr_x/Re_x^2 are respectively 6.22×10^3, 9.6×10^7, 2.49).

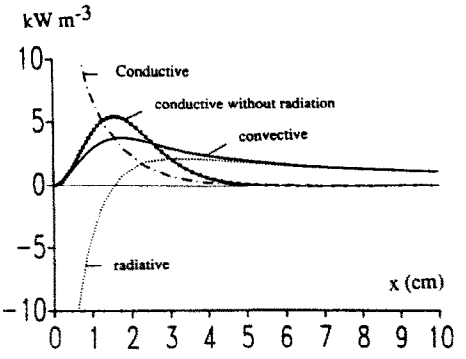

FIG. 5. Distributions of conductive diffusion ($\lambda(\partial^2 T/\partial y^2)$), radiative dissipation ($-(\partial q^R/\partial y)$) and convective term at the location $x = x_{max}$ in the same conditions as in Fig. 4.

of y_{max}, corresponding to $\eta = 40$ and denote it by $y_{\eta=40}$:

$$y_{max} = \frac{40 x_{max}}{\left(\frac{Gr_x}{4}\right)^{1/4}} = y_{\eta=40}. \quad (12)$$

This choice will be discussed later.

The radiation penetration length is characterized by the fact that the radiative dissipation $-\partial q^R/\partial y$ tends to zero at this distance from the wall. The radiative dissipation distributions at different locations $x = x_{max}/10$, $x_{max}/4$, $x_{max}/2$, x_{max} are presented in Fig. 4 for pure water vapour at $T_\infty = 600$ K and $u_\infty = 0.5$ m s^{-1} and a wall at $T_w = 650$ K, $\varepsilon_w = 0.2$. The peak value of radiative dissipation is located at a distance from the wall corresponding to the thermal boundary layer thickness for mixed convection without fluid radiation (see Fig. 6 which presents the temperature and velocity profiles in the same conditions as Fig. 4). The radiative dissipation decreases to 1% of its peak value at nearly the same distances from the wall: $y = 0.54$, 0.55, 0.56, 0.60 m for $x = x_{max}/10$, $x_{max}/4$, $x_{max}/2$, x_{max}, respectively. The radiation penetration length does not seem to have much dependence on x.

In general, the medium absorbs more than it emits, but there exists a small region near the heating wall where the medium emits more than it absorbs. In the immediate vicinity of the wall, $(-\partial q^R/\partial y)$ grows quasi-linearly from a finite negative value (not shown on Fig. 4 for scale convenience). In fact, the medium temperature in the region where $(-\partial q^R/\partial y)$ is negative is close to the wall temperature, the cold medium far away from the wall is heated by radiation from the medium in the vicinity of the wall. This phenomenon has also been observed in previous studies [13, 15]. Furthermore, the strong radiative absorption by the medium in the vicinity of the wall leads to large conductive diffusion which balances the negative radiative dissipation in this region. Figure 5 shows the radiative dissipation, the conductive diffusion and the convective term in the energy equation vs the coordinate y. The distributions of conductive diffusion in the cases considering and neglecting medium radiation are significantly different.

4.3. *Interaction of radiation and mixed convection*

Figure 6 presents the temperature and the two components of velocity profiles at $x = x_{max}$ for pure water vapour at the same conditions as in Fig. 4. The results for pure natural, pure forced and mixed convection without radiation are also illustrated in Fig. 6, for the same wall and fluid conditions, in order to show the interaction between radiation, buoyancy force and the effect of external forced flow. It is found that the gas radiation significantly increases the temperature gradient in the vicinity of the wall, wall conductive flux and also the width of the thermal perturbation region (Fig. 6(a)). The temperature for mixed convection approaches the ambient temperature T_∞ more rapidly without radiation than with it.

The radiative heating of the fluid in a thick layer

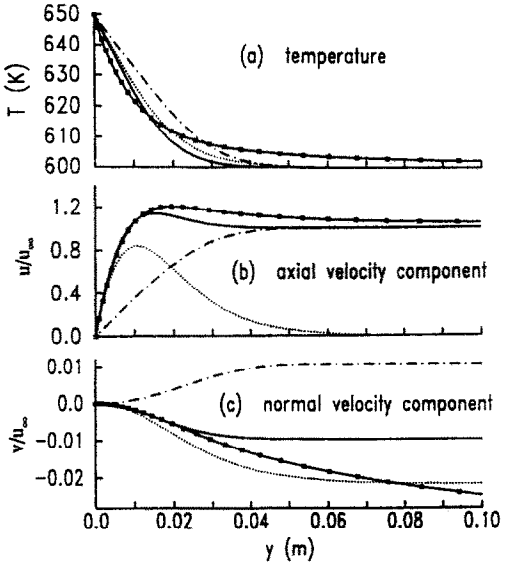

FIG. 6. Temperature and velocity profiles at $x = x_{max}$ for mixed convection with (—⊟—) and without radiation (——), pure forced convection (— · —), and pure natural convection (----) in the same conditions as in Fig. 4.

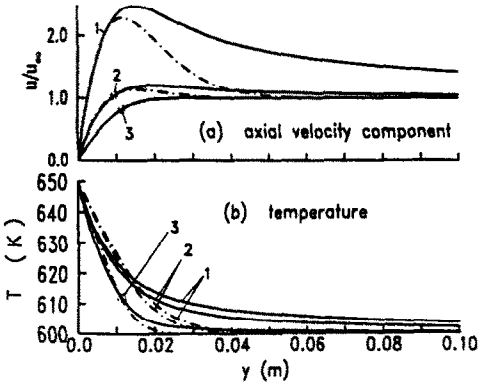

FIG. 7. Temperature and velocity profiles at $x = x_{max}$ for mixed convection with (——) and without radiation (—·—), at different values of (1) $u_\infty = 0.2$, (2) $u_\infty = 0.5$, (3) $u_\infty = 2.0$ m s^{-1} for pure water vapour with the conditions $T_w = 650$ K, $\varepsilon_w = 0.5$, $T_\infty = 600$ K (Re_x values are respectively 2.49×10^3, 6.22×10^3, 2.49×10^4).

induces a buoyancy force up to the same distance from the wall. This is observed in the axial velocity profiles (Fig. 6(b)). The fluid radiation assists the natural convection flow. This fact allows us to choose the value of y_{max} given by equation (12).

For pure forced convection, the external forced flow is dragged by the viscous force at the wall. Therefore, a second flow several orders of magnitude smaller crosses the boundary layer in the y-direction and the normal velocity component is then positive (Fig. 6(c)). Opposingly, a buoyancy force drives a flow along the wall in the x-direction: a secondary flow is needed to supply the flow along the wall, so the normal velocity component for pure natural convection is negative. For mixed convection without radiation the normal velocity component profile is located between those of pure forced and pure natural convection. The direction of the normal velocity component depends on the relative effects of the buoyancy force and forced flow.

Temperature and axial velocity are shown in Fig. 7 for mixed convection with and without gas radiation in the same conditions as in Fig. 6 except for the infinity velocity u_∞, which is taken to be 0.2, 0.5, 2 m s^{-1}, respectively. The effect of radiation increases both temperature and velocity when u_∞ decreases. This is to be expected, since the decrease of u_∞ is equivalent to an increase of the relative effect of buoyancy force on forced convection flows. On the other hand, gas radiation in the case of high u_∞ values no longer affects the velocity distribution, but slightly modifies the temperature field (see Fig. 7, curve 3). Heat transfer coefficients in the three cases are presented in Fig. 8 for mixed convection with and without gas radiation. The conductive heat transfer coefficient is calculated from

$$h_C = \frac{-\lambda\left(\frac{\partial T}{\partial y}\right)_{y=0}}{T_w - T_\infty} = -\lambda\left(\frac{\partial \theta}{\partial y}\right)_{y=0} \tag{13}$$

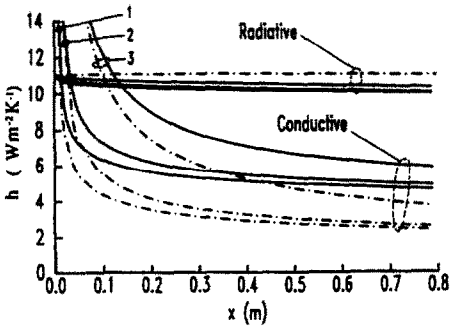

FIG. 8. Conductive and radiative transfer coefficients vs x; same conditions and symbols as in Fig. 7.

where λ is the thermal conductivity of the gas mixture. The radiative transfer coefficient is deduced from the wall radiative flux

$$h_R = \frac{q_w^R}{T_w - T_\infty}. \tag{14}$$

When gas radiation is not considered, the above equation is written as

$$h_R' = \frac{\varepsilon_w \sigma (T_w^4 - T_\infty^4)}{T_w - T_\infty} \tag{15}$$

where σ is the Stefan–Boltzmann constant. Gas radiation enhances the conductive flux. This increase is more significant when u_∞ is small. At $x = x_{max}$ the conductive transfer coefficient is doubled by the gas radiation for $u_\infty = 0.2$ m s^{-1} and increases by 54% at $u_\infty = 2$ m s^{-1}. The wall radiative flux is diminished when the gas radiation is considered: the radiating medium near the wall at a temperature above T_∞ increases the contribution of incident radiative flux to the wall above that for the case of the transparent medium. The variation of h_R with u_∞ is not as significant as that of h_C; h_R increases slightly with u_∞ but the difference $h_R' - h_R$ decreases with u_∞.

Results on temperature, normal velocity component and radiative dissipation profiles at $x = x_{max}$ are reported in Fig. 9 for different values of the wall emissivity for the case of pure water vapour at conditions $T_\infty = 600$ K, $u_\infty = 0.5$ m s^{-1} and $T_w = 650$ K. The wall emissivity varies from $\varepsilon_w = 0.01$ (very reflecting wall) to 1.0 (black wall). In the first case, the wall radiation is very small, hence the flow is less heated than at a high emissivity; temperature, u velocity component and radiative dissipation increase with the wall emissivity. The heat transfer coefficients corresponding to the above three cases are presented in Fig. 10. The conductive transfer coefficient h_C increases when ε_w decreases. Compared to mixed convection without gas radiation, h_C increases by more than 110% for $\varepsilon_w = 0.01$, about 90% for $\varepsilon_w = 0.2$ and less than 8% for $\varepsilon_w = 1.0$. In fact, when the wall is more reflecting, the optical path length of the gas is effectively stretched: the interaction of fluid radiation with convection is strengthened.

A computation has also been carried out for the

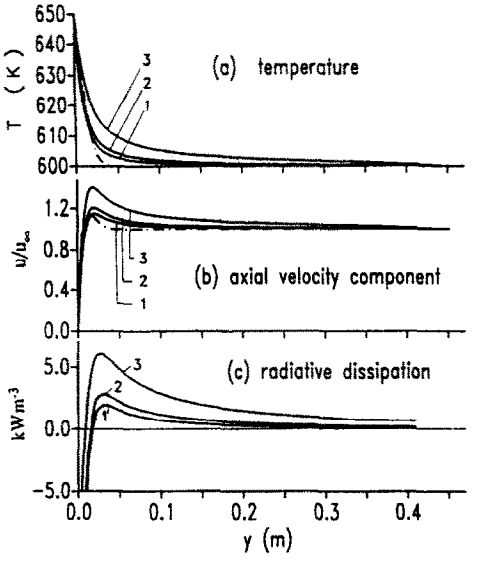

FIG. 9. Temperature, velocity and radiative dissipation profiles at $x = x_{max}$ for mixed convection with (——) and without radiation (—·—), at different wall emissivities (1) $\varepsilon_w = 0.01$, (2) $\varepsilon_w = 0.2$, (3) $\varepsilon_w = 1.0$ for pure water vapour at conditions $T_w = 650$ K, $T_\infty = 600$ K, $u_\infty = 0.5$ m s^{-1} (Re_x, Gr_x, Gr_x/Re_x^2 in the three cases are identical to those in Fig. 4).

different H_2O–air mixtures in the case of $T_w = 650$ K, $\varepsilon_w = 0.2$, $u_\infty = 0.5$ m s^{-1}, $T_\infty = 600$ K. The value of the H_2O molar fraction x_{H_2O} has been varied from 0 to 1. Results about conductive and radiative transfer coefficients are shown in Fig. 11 for the different values of x_{H_2O}. When the water vapour molar fraction in the mixture increases, the conductive transfer coefficient increases and the radiative transfer coefficient decreases, since the effect of the fluid radiation becomes more significant when the concentration of the absorbing and emitting gas species increases. Fluid radiation generally strengthens conductive transfer. On the other hand the fluid composition is changed with the variation of x_{H_2O}, and the conductivity,

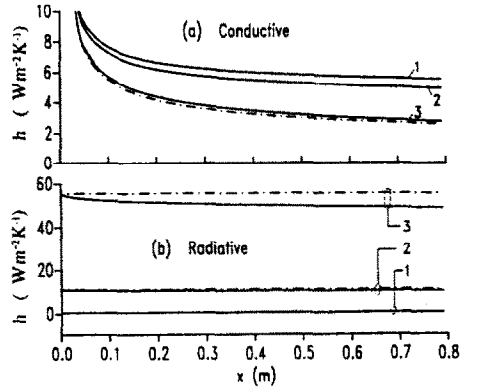

FIG. 10. Conductive and radiative heat transfer coefficients vs x and wall emissivities; same conditions and symbols as in Fig. 9.

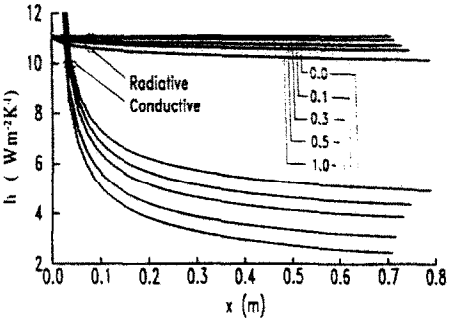

FIG. 11. Conductive and radiative heat transfer coefficients vs x and molar fraction of water vapour at $T_w = 650$ K, $\varepsilon_w = 0.2$, $T_\infty = 600$ K, $u_\infty = 1.0$ m s^{-1}.

Prandtl number and other physical properties of the fluid are changed also.

It should be pointed out that fluid radiation decreases the wall radiative flux but increases the convected enthalpy of the fluid.

In engineering problems related to coupled radiation and mixed convection, one wishes to estimate whether fluid radiation and mixed convection are both important, or which one is dominant. Such a criterion should account for the real gas radiation which does not only depend on the temperature but also depends on the medium opacity. We propose the following dimensionless parameter:

$$R = \frac{\alpha_e(\delta)\sigma(T_w^4 - T_\infty^4)}{h_c'(T_w - T_\infty)} \tag{16}$$

where h_c' and $\alpha_e(\delta)$ are respectively the conductive transfer coefficient and the effective medium absorptivity associated to the thermal boundary layer thickness δ without fluid radiation. The effective absorptivity is given by

$$\alpha_e(\delta) = 1 - \tau_e = \frac{\pi \int_0^\infty [1 - \tau_\nu(\delta)][I_\nu^b(T_w) - I_\nu^b(T_\infty)]\,d\nu}{\sigma(T_w^4 - T_\infty^4)}. \tag{17}$$

The parameter R is related to the ratio between near-wall radiative to gas transfer and conductive transfer. On the other hand, the relative enhancement of conductive heat transfer, due to gas radiation, is $R_q = (q_c - q_c')/q_c'$ where q_c and q_c' are respectively the conductive fluxes when considering and neglecting gas radiation, respectively. The ratio R_q R vs x is shown in Fig. 12 in various conditions. It is seen that this ratio is practically independent on x for each calculation, except near the leading edge. For engineering applications, the quantity $0.3R$ is a crude estimation of conductive flux enhancement due to gas radiation. Depending on the required accuracy, this criterion shows easily if an exact coupled resolution is necessary or not for a given problem. It is worth noticing that the wall emissivity ε_w does not appear in equation (16) since we are especially concerned with the effects of

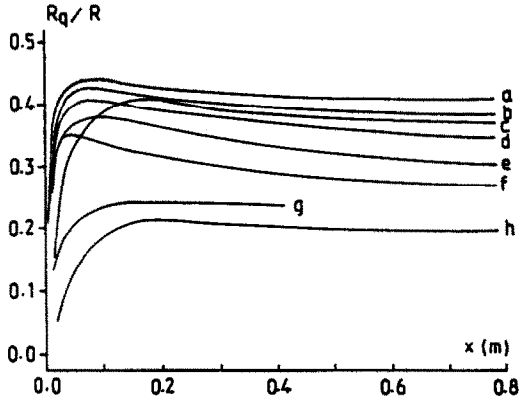

FIG. 12. Dependence of conductive flux enhancement due to gas radiation on the dimensionless parameter R in various conditions

	Curve							
	a	b	c	d	e	f	g	h
T_w (K)	650	650	650	650	650	650	450	850
T_∞ (K)	650	600	600	600	600	600	400	800
ε_w	0.2	0.2	0.2	0.2	0.2	0.2	0.5	0.5
u_∞ ($m s^{-1}$)	0.5	2.0	0.5	0.5	0.5	0.2	1.0	1.0
x_{H_2O}	0.1	1.0	0.3	0.5	1.0	1.0	1.0	1.0

radiation on the conductive flux near the wall. Moreover, Fig. 10 shows that the conductive flux increases with the wall reflectivity $(1-\varepsilon_w)$. This is a result of the growing magnitude of radiative transfer from gas layers far from the wall to the wall adjacent layer. Consequently, the ratio R_q/R decreases with ε_w as it is shown on Fig. 12 (curves h and g). A multiplicative factor $(2-\varepsilon_w)$, accounting for wall reflection of gas radiation, could be introduced in equation (16) for a more precise analysis.

5. CONCLUSION

Coupled radiation and mixed convection heat transfer in an absorbing and emitting real gas mixture along a vertical isothermal plate has been investigated using an implicit finite-difference technique with a marching procedure for the solution of conservation equations, and a random statistical narrow-band model with the Curtis–Godson approximation for the treatment of the radiative transfer part.

The radiation penetration length at atmospheric pressure is found to be of the order of one pure H_2O equivalent metre in the case of mixed convection. This length corresponds to the region within which the temperature and velocity fields are affected by the gas radiation, and is of one order of magnitude larger than the boundary layer thickness for mixed convection without fluid radiation. The boundary conditions at infinity should be carefully examined.

Fluid radiation enhances the effect of the buoyancy force, particularly far away from the wall. The thermal and dynamic flow fields are significantly modified by fluid radiation when natural convection predominates.

The interaction of radiation with mixed convection increases with the decrease of the wall emissivity and with the increase of the radiating species in the gas mixture.

Fluid radiation strengthens the wall conductive transfer and weakens the wall radiative flux. The relative change in conductive flux is more significant than in radiative flux.

A dimensionless parameter R is introduced to characterize radiative effects on wall conductive flux. Calculations in various conditions show that the relative enhancement of conductive flux by gas radiation can be crudely estimated from this parameter.

REFERENCES

1. R. D. Cess, The interaction of thermal radiation with free convection heat transfer, *Int. J. Heat Mass Transfer* **9**, 1269 (1966).
2. V. S. Arpaci, Effect of thermal radiation on the laminar free convection from a heated vertical plate, *Int. J. Heat Mass Transfer* **11**, 871 (1968).
3. S. Hasegawa, R. Echigo and K. Fukuda, Analytical and experimental studies on simultaneous radiative and free convective heat transfer along a vertical plate, *Heat Transfer—Jap. Res.* **1**, 21 (1968).
4. E. H. Cheng and M. N. Özisik, Radiation with free convection in an absorbing, emitting and scattering medium, *Int. J. Heat Mass Transfer* **15**, 1243 (1972).
5. W. G. England and A. F. Emery, Thermal radiation effects on the free convection boundary layer of an absorbing gas, *J. Heat Transfer* **91**, 37 (1969).
6. J. L. Novotny, J. R. Lloyd and J. D. Bankston, Local nonsimilarity applied to free convection boundary layers with radiation interaction, *Prog. Aeronaut. Astronaut.* **39**, 309 (1975).
7. R. D. Cess, Radiation effect upon boundary layer flow of an absorbing gas, *J. Heat Transfer* **86**, 469 (1964).
8. J. B. Bergquam, Heat transfer by convection and radiation in laminar boundary layer flow, *J. Heat Transfer, Proc. 5th Int. Heat Transfer Conf.*, Vol. 1, p. 83 (1974).
9. C. L. Tien and J. E. Lowder, A correlation for total band absorption of radiative gases, *Int. J. Heat Mass Transfer* **9**, 698 (1966).
10. S. De Soto, Coupled radiation, conduction, and convection in entrance region flow, *Int. J. Heat Mass Transfer* **11**, 39 (1968).
11. A. T. Wassel and D. K. Edwards, Molecular gas radiation in a laminar or turbulent pipe flow, *J. Heat Transfer* **98**, 101 (1976).
12. Y. Yamada, Combined radiation and free convection heat transfer in a vertical channel with arbitrary wall emissivities, *Int. J. Heat Mass Transfer* **31**, 429 (1988).
13. A. Soufiani and J. Taine, Application of statistical narrow-band model to coupled radiation and convection at high temperature, *Int. J. Heat Mass Transfer* **30**, 437 (1987).
14. A. Soufiani, J. M. Hartmann and J. Taine, Validity of band-model calculations for CO_2 and H_2O applied to radiative properties and conductive–radiative transfer, *J. Quant. Spectrosc. Radiat. Transfer* **31**, 243 (1985).
15. L. Zhang, A. Soufiani and J. Taine, Spectral correlated and non-correlated radiative transfer in a finite axisymmetric system containing an absorbing and emitting real gas–particle mixture, *Int. J. Heat Mass Transfer* **31**, 2261 (1988).

16. R. M. Goody, *Atmospheric Radiation*, Chap. 4, pp. 122–170. Clarendon Press, Oxford (1964).
17. W. Malkmus, Random Lorentz band model with exponential-tailed S-1 line-intensity distribution, *J. Opt. Soc. Am.* **57**, 323 (1967).
18. C. B. Ludwig, W. Malkmus, J. E. Reardon and A. L. Thompson, *Handbook of Infrared Radiation from Combustion Gases*, NASA SP-3080. Scientific and Technical Information Office, Washington, DC (1973).
19. L. S. Bernstein, Band model parameters for the parallel bands of linear triatomic molecules—I. Theory, *J. Quant. Spectrosc. Radiat. Transfer* **23**, 157 (1980).
20. S. J. Young, Evaluation of nonisothermal band models for H_2O, *J. Quant. Spectrosc. Radiat. Transfer* **18**, 29 (1977).
21. J. M. Hartmann, R. Levi Di Leon and J. Taine, Line by line and narrow band statistical model calculations for H_2O, *J. Quant. Spectrosc. Radiat. Transfer* **32**, 119 (1984).
22. N. L. Godson, The evaluation of infrared radiative fluxes due to atmospheric water vapor, *Q. J. Met. Soc.* **79**, 367 (1953).
23. S. J. Young, Nonisothermal band model theory, *J. Quant. Spectrosc. Radiat. Transfer* **18**, 1 (1977).
24. F. G. Blottner, Introduction to computational techniques for boundary layers, Report Sand 79-0893, pp. 42–43, Sandia Laboratories, Albuquerque, New Mexico (1981).
25. L. Zhang, Transferts radiatifs corrélés dans des gaz chauds; couplage avec la convection mixte laminaire. Validation d'une technique expérimentale, Thèse de Doctorat, Ecole Centrale Paris, Châtenay–Malabry, France (1989).
26. S. Ostrach, An analysis of laminar free-convection flow and heat transfer about flat plate parallel to the direction of generating body force, NACA Rept. 1111 (1953).
27. W. M. Kays and M. E. Crawford, *Convective Heat and Mass Transfer*. McGraw-Hill, New York (1980).
28. M. S Raju, X. Q. Liu and C. K. Law, A formulation of combined forced and free convection past horizontal and vertical surfaces, *Int. J. Heat Mass Transfer* **27**, 2215 (1984).
29. R. C. Reid and T. K. Sherwood, The properties of gases and liquids. In *Chemical Engineering Series* (2nd Edn). McGraw-Hill, New York (1966).
30. Y. S. Touloukian, P. E. Liley and S. C. Saxena. *Thermophysical Properties of Matter*. Vol. 3. IFI/Plenum, New York/Washington (1970); Y. S. Touloukian, S. C. Sexena and P. Hestermans, *Thermophysical Properties of Matter*, Vol. 3. IFI/Plenum, New York/Washington (1975).

COUPLAGE DU RAYONNEMENT ET DE LA CONVECTION MIXTE LAMINAIRE DANS UN MÉLANGE DE GAZ RÉELS ABSORBANTS ET ÉMETTEURS LE LONG D'UNE PLAQUE PLANE VERTICALE

Résumé—Les propriétés radiatives du mélange sont obtenues par un modèle statistique aléatoire à bandes étroites et l'approximation de Curtis–Godson. Une technique de différences finies, developpée pour cette étude, est utilisée pour résoudre d'une mainière couplée les équations de conservation de la masse, de la quantité de mouvement et de l'énergie. Un excellent accord entre nos résultats et ceux d'autres auteurs est obtenu dans les cas de la convection naturelle, de la convection forcée et de la convection mixte considérées sans rayonnement du fluide. L'examen des conditions aux limites à l'infini conduit à une longueur de pénétration du rayonnement équivalente à un mètre de vapeur d'eau pure à pression atmosphérique, qui est d'un ordre de grandeur plus grande que l'épaisseur de la couche limite en convection mixte sans couplage. La comparaison des résultats avec et sans rayonnement dans diverses conditions montre que le rayonnement du gaz augmente l'effet de la convection naturelle sur la température, la vitesse, et le coefficient conducto-convectif, mais diminue le flux radiatif à la paroi. Un paramètre adimensionné R est introduit afin de permettre une estimation rapide mais grossière de l'augmentation du flux conductif à la paroi due au rayonnement du fluide.

GEKOPPELTER WÄRMEAUSTAUSCH DURCH STRAHLUNG UND LAMINARE MISCHKONVEKTION IN EINER ABSORBIERENDEN UND EMITTIERENDEN MISCHUNG REALER GASE ENTLANG EINER VERTIKALEN PLATTE

Zusammenfassung—Der Anteil der Wärmeübertragung durch Strahlung wird unter Anwendung eines statistischen Zufallsmodells im Schmalbandbereich und der Curtis–Godson-Näherung behandelt. Ein für diese Untersuchungen entwickeltes Finite-Differenzen-Verfahren wird zur Lösung der Erhaltungsgleichungen für Masse, Impuls und Energie in gekoppelter Weise angewendet. Eine hervorragende Übereinstimmung zwischen unseren Finite-Differenzen-Lösungen und denen anderer Autoren wird festgestellt für die Fälle der reinen natürlichen Konvektion ohne Strahlung. Die Untersuchung der Randbedingungen im Unendlichen zeigt, daß die Strahlungseinwirkungslänge bei Atmosphärendruck von der Größenordnung eines Meters Wasseräquivalent ist. Dieses ist eine Größenordung größer als die Grenzschichtdicke bei gemischter Konvektion ohne Strahlung. Vergleiche der Ergebnisse mit und ohne Strahlung bei berschiedenen Bedingungen zeigen, daß die Fluidstrahlung den Einfluß der Auftriebskräfte verstärkt, die Temperatur, Geschwindigkeit und Wärmeübertragung durch Leitung an der Wand erhöht, aber die Strahlungswärmestromdichte an der Wand erniedrigt. Es wird ein dimensionsloser Parameter R eingeführt, um eine genaue Berechnung der Erhöhung der Wärmestromdichte durch Leitung an der Wand aufgrund der Strahlung zu ermöglichen.

СВЯЗАННЫЕ ИЗЛУЧЕНИЕ И ЛАМИНАРНАЯ СМЕШАННАЯ КОНВЕКЦИЯ В ПОГЛОЩАЮЩЕЙ И ИЗЛУЧАЮЩЕЙ ГАЗОВОЙ СМЕСИ, ОБТЕКАЮЩЕЙ ВЕРТИКАЛЬНУЮ ПЛАСТИНУ

Аннотация—С использованием вероятностно-статистической узкополосной модели и приближения Куртиса–Годсона исследуется лучистый перенос. Для решения связанных уравнений сохранения массы, импульса и энергии применяется разработанный для данного исследования неявный метод конечных разностей. Обнаружено очень хорошее согласие между решениями, полученными конечно-разностным методом в данной работе и в работах других авторов для случаев чисто естественной, чисто вынужденной и смешанной конвекции в отсутствие излучения. Изучение граничных условий на бесконечности показывает, что при атмосферном давлении излучение проникает на глубину, которая примерно равна одному эквивалентному метру в чистой H_2O и которая на порядок величины больше толщины пограничного слоя при смешанной конвекции без излучения жидкости. Сравнение результатов, полученных для случаев с излучением и без него в различных условиях показывает, что излучение жидкости усиливает эффект подъемных сил, увеличивает температуру, скорость и кондуктивный теплоперенос у стенки и уменьшает излучающий тепловой поток на стенке. Для грубой оценки увеличения кондуктивного теплового потока на стенке, обусловленного излучением, вводится безразмерный параметр R.